



An analytical solution for the geometric broken characteristics of the overlying strata and its physical modeling study in longwall coal mining

Shengli Yang^{1,2} · Gaofeng Song³ · Jinghu Yang^{1,2}

Received: 3 May 2018 / Accepted: 22 January 2020 / Published online: 1 February 2020
© Saudi Society for Geosciences 2020

Abstract

The broken positions of the overlying strata might lead to different geometric configurations of the caving overburden and also have an impact on the coal mine pressure behaviors and dynamic mine hazards in the open face area. This paper has developed a roof failure analytical model combining the beam on the elastic foundation theory and the cantilever beam theory. The model gives the analytical solutions for the roof broken positions, rock broken angle, and strata broken angle. The results show that (1) the roof broken position is moved forward ahead of the face with decreasing feature coefficient, (2) the strata broken angle is not only influenced by the feature coefficient but also in direct proportion to the ratio of the uniformly distributed load over the roof stiffness, and (3) the theoretical model is capable of simulating the three geometric configurations of the disturbed overlying strata, i.e., the regular trapezoid-shaped, rectangular-shaped, and inverted trapezoid-shaped configurations. An improved physical modeling study is performed in order based on the deviation analysis on the conventional physical modeling studies. The physical model physically realistically reproduces three of the abovementioned geometric caving configurations predicted by the analytical model.

Keywords Strata movement · Cantilever beam theory · Beam on elastic foundation theory · Physical modeling · Roof broken position · Strata broken angle

Background and problem statement

As a major source of energy, coal remains the dominant fuel in China's energy mix and accounted for about 62% of national energy consumption in 2016 (BP 2017). However, affected by the downward pressure on economic growth and the excess production capacity, the Chinese coal industry has entered a recession phase marked by the excess supply of coal and dramatically declines of coal price and corporate profits at the end

of the booming golden 10 years in 2012 (Liu and Luan 2015; Gao 2012). Since then, China has started the overcapacity-cutting and production-optimizing operations including annexation, reorganization, transformation, and upgrading of coal enterprises. As a result, a total of 14 large-scale coal bases across the country were recognized, each of which has an annual production of more than 100 Mt. The 14 coal bases combined contribute over 90% of the total coal production in Chinese coal industry, and this is expected to increase to 95% by 2020 as the overcapacity cuts continue (National Energy Administration 2016; Qian et al. 2018; Wang et al. 2016a). Of those, Shandong, Shanbei, Huanglong, and Xinjiang are four of the most promising coal bases with abundant proven reserves and preferable geological and mining conditions, compared with depleting resources and large depth of occurrence in the rest of the 10 coal bases. A large amount of 6–9 m high coal seams deposits in the abovementioned four major coal bases. Due to the unfavorable cavability of the coal seam, most of the seams are mined using the extra-large-cutting-height longwall mining method, which is defined as cutting height larger than 7 m in this paper (Wang and Pang 2018)

Responsible Editor: Murat Karakus

✉ Gaofeng Song
song.gaofeng@ncut.edu.cn

¹ School of Energy and Mining Engineering, China University of Mining & Technology Beijing, Beijing 100083, China

² Research Center of Top-coal Caving Mining in Coal Mining Industry, Beijing 100083, China

³ School of Civil Engineering, North China University of Technology, Beijing 100144, China

(note that the conventional large-cutting-height longwall face is larger than 3.5 m). The 6- and 7-m longwall mining applications have been extensively practiced in the industry with significantly improved productivity and efficiency. However, the goal is to extract the 9-m high full seam and further increase the coal recovery. With the improvement of mining equipment and hazard management in the open face area, the largest mining height in China has further increased to 8 m in recent years (Wang et al. 2017a; Yang 2017). Currently, Shangwan coal mine in Shendong coal base is testing the 8.8-m single-cut longwall mining method.

Large-cutting-height longwall mining system has long been recognized as a better mining method over top coal caving and multiple slicing mining methods for extracting the thick coal seam in terms of coal recovery, safety, productivity, and efficiency (PENG and CHIANG 1984; Wang 2009; Wang and Zhong 2008; Meng et al. 2014; Song et al. 2015). Extra-large-cutting-height longwall mining, on the other hand, has further improved the benefits and advantages of longwall mining and is considered to be the most suitable mining method for recovering the 6–9 m coal seam in the four major coal bases. As compared with coal faces with regular mining height, extra-high longwall face may experience the most severe and dynamic roof caving-related problems and mine hazards in the open face area (Han et al. 2017; Zhang and Li 2017; Wang et al. 2016b). Field trips also confirm that very violent periodic roof weightings may occur over a larger area along face for a longer duration. Face collapse extends a larger height and deeper depth on the face wall and is followed by immediate roof fall ahead of supports. Power supports normally see tremendous high pressure level or even a massive impact loading. In some cases, failure of power supports and inrush of water/sand into the face area may occur and result in the cease of mining operations and fatal injuries of miners (Research Group of National Key Basic Research Program of China 2017; Fan et al. 2016). This is largely due to the fact that this mining system advances at a quicker rate and creates a massive vacant mined-out area behind the face. Figure 1 plots the face collapse and support failure captured in the high-seam longwall faces.

Research hypothesis, goal, and specific objectives

The stability and performance of the face and supports are the major ground control concerns in the open face area when mining thick coal seams (Song et al. 2017; Song and Chugh 2018). A number of studies have repeatedly reported that a lack of adequate working resistance of the shield legs might be responsible for the poor performance or failure of face and supports (Mondal et al. 2017; Verma and Deb 2010; Verma and Deb 2007; Ghose 2003). Therefore, efforts to increase the

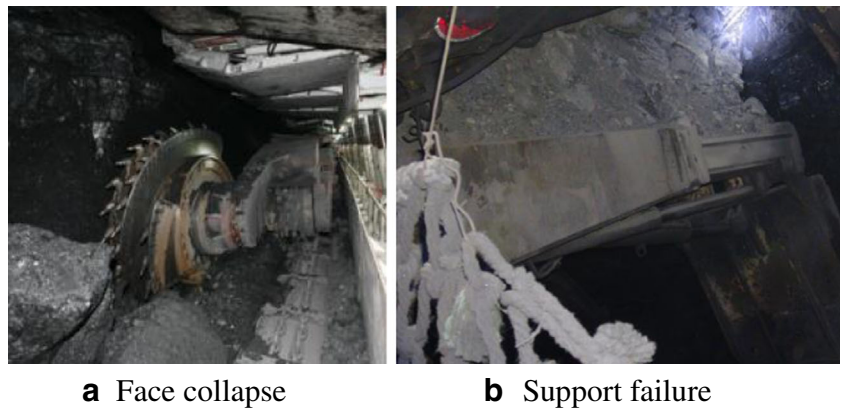
load capacity of the supports have been studied for decades with improved ground control in the open face area. Currently, the 8.8-m support installed in Shangwan coal mine has the largest load capacity of 26,000 kN. The authors believe that the dynamic movement of the strong, hard, and competent roof above the face and supports might be the fundamental reason for the mine hazards in the open face area. A better understanding of the behaviors of the strong roof, therefore, is helpful for solving the ground control problems and also the normal functioning of the shields.

Previous studies have agreed on the comments that the broken position of the roof might be highly influential to the mine pressure behaviors in the face area (Wang et al. 2017b; Wang and Pang 2016; Wang and Pang 2015). The stability of the face and support would be better off if the roof breakage occurs right behind the support instead of along the faceline or ahead of the face (see Fig. 2). When dislocation of the strong and massive roof occurs ahead of the faceline, it may exert an impact load on the face and supports; as the face advances to the dislocation position, failure or crush of the support may occur if the shield cannot provide adequate pressure to the roof. By contrast, when the hanging roof falls down regularly behind the support, the face area may have the least negative impacts of mine hazards. This is also why the coal mines utilize the induced blasting methods to cave the thick and hard roof that overhangs a large area behind the face, so that the complete failure of the support or strong wind blowouts can be avoided (Yang 2017; Zhang and Li 2017; Mondal et al. 2017; Roy et al. 2003). It is also well agreed that, with the increase of support load capacity and stiffness, the roof broken position is tended to be moved towards the gob side direction. The broken position of the main roof may also have an influence on the broken positions of the weaker roof layers above the main roof.

On the other hand, most of the physical models have successfully reproduced the situation that roof breakage occurs behind the supports, with a trapezoid-shaped geometric configuration of the disturbed overburden strata after the finish of face advance. However, the roof breaks ahead of the face has not been reported in the previous physical modeling studies. In other words, the regular physical modeling studies have not reproduced the reversed trapezoid-like roof caving configuration (roof breaks ahead of coal seam or the lower roof layer) and the rectangular roof caving configuration (roof breaks at the same location for different layers). The authors believe this is mainly because the mechanical properties of the strata are not scaled down correctly to those of the physical materials according to the principle of similarity.

A better scientific understanding of the broken position of the roof with relation to the longwall face is necessary to effectively mitigate the roof caving-related problems and improve the ground control in the face area, so that the productivity and safety can further be improved. This paper is

Fig. 1 Face failure and support crush observed in the longwall face



therefore focused on analysis of the roof breakage positions, the corresponding geometric configuration of the caving overlying strata above the gob, and its impacts on the mine pressure behaviors in the face area. This paper has four goals: (1) develop an analytical model using the cantilever beam theory and beam on elastic foundation theory for analyzing the broken positions of the strong and hard main roof as well as the above weaker roof layers and determining the geometric configurations of the disturbed overburden, (2) provide a case study for application of the proposed model, (3) perform deviation analysis on the conventional physical models and identify the dominant governing parameters that influence the roof caving characteristics, and (4) perform physical modeling studies to reproduce the different caving configurations described by the analytical model and the associated mine hazards.

Review of pertinent literature

The movement of the overlying strata has been extensively studied in the previous literatures. Qian proposed a “Voussoir beam” model in the 1960s that describes the structural characteristics of the disturbed overlying strata (Qian 1983; Qian and Li 1982). This model also provides a criterion for the sliding and rotation failures of the main roof. The “Key

Strata” theory was presented in the 1990s which defines the hard, massive, and competent roof strata as the key/sub-key strata that are strong enough to influence or determine the movement of the above weaker strata up to the ground surface (Qian et al. 1996). The strata movement has also been studied using the “short Voussoir beam” model for the shallow coal seams with thick unconsolidated formation and thin-bedrock geological conditions (Huang et al. 1999). With these models, a broad-based observation on the development of the “caved zone,” “fractured zone,” and “continuous deformation zone” above the mined-out area was provided. The behaviors of the main roof have also been perused. The classical plate theory (Jia and Huo 1999) and beam theory (Qian 1981) were used to analyze the stress and displacement of the strong and hard roof above the foundation (foundation defined as the immediate roof and coal seam in this paper). The foundation, however, is assumed rigid in their models, which might be too rigorous for analyzing the complex breakage of the roof in a real mine. Li et al. (2007) developed a series of moment equations to study the breakage and energy release of the strong roof (Li et al. 2007). The immediate roof and coal seam below the strong roof was considered as elastic in their model. Wang et al. (2014), Wang and Wang (2015) proposed a dynamic simulation method for determining the required load capacity of the shields for the thick coal seams (Wang et al. 2014; Wang and Wang 2015). He also recommended a list of impact

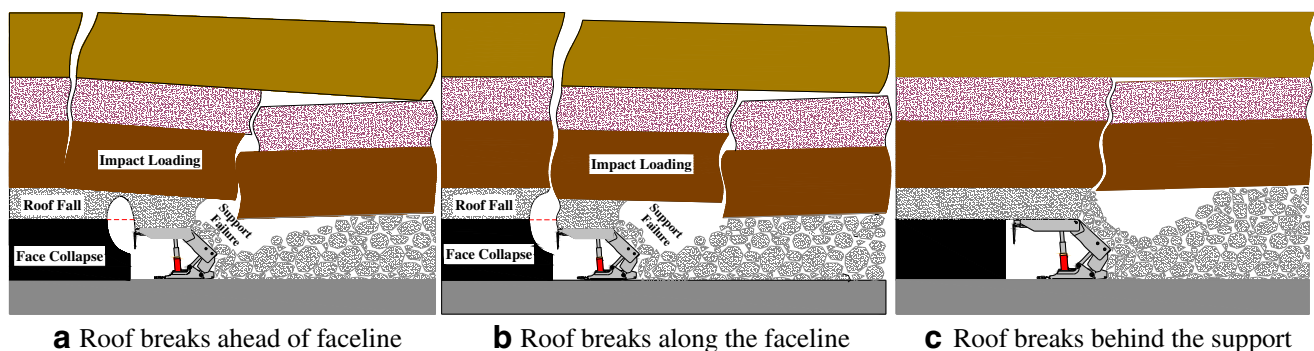


Fig. 2 A schematic of the mine hazards in the face area including the face collapse followed by roof fall ahead of the support, impact loading of the main roof and support failure

loading coefficients for the shield supports under different mining methods and different roof classifications. Pan et al. (2012a, b, 2013), Pan and Gu (2014) utilized the statically indeterminate differential equation of deflection curve to study the deflection, shearing force, bending moment, and energy change of the competent roof during the first and periodic roof weightings, and how these parameters vary with the overburden loads, support capacity, foundation stiffness, and periodic roof weighting intervals (Pan et al. 2012a; 2012b; 2013; Pan and Gu 2014). In their models, the roof breaks 6–8 m ahead of the face. The previous analytical models provide a theoretical basis for the prediction of the occurrence of roof weightings and the determination of the power support load capacity. However, the broken positions of the main roof as well as a few weaker roof strata above the main roof were not considered in depth.

Physical modeling of the roof caving behaviors has been frequently documented in the previous studies. Song et al. (2015) studied the dynamic movement of the roof and the extension of caved and fractured zone heights with face advance (Song and Yang 2015). Li et al. (2015) analyzed the characteristics of acoustic emission signals during the failure process of the hard roof. The maximum AE energy was found at the position where the roof breakage occurs (Li et al. 2015). Xu et al. (2017) reproduced the trapezoid-like configuration of the disturbed overburden strata using the physical modeling study. An overall decreasing trend of the fracture space from the model bottom to the top was observed, which is the most typical result of the conventional physical modeling studies (Xu et al. 2017). Yang et al. (2017) developed a physical modeling rig to study the roof movement in the shallow-buried thin-bedrock coal seams and its effects on the stability of the face and performance of the supports (Yang et al. 2017). The results show that the impact load on the support at roof weighting is two times of the support working resistance during the normal advance of longwall face. The short Voussoir beam was also reproduced in his physical model. Most of the physical models, however, cannot reproduce the case that roof breaks ahead of or along the face, the geometric configuration of the disturbed overburden strata in the regular physical models is therefore trapezoid-shaped, instead of reversed trapezoid-like or rectangular-like.

The previous works have largely improved our understandings on the movement and dynamic behaviors of the roof including the structural forms of the strong roof after failure and the analysis of internal force and deflection of the roof ahead of and behind the face. The broken position of a single roof layer (say the main roof) and the dynamic load on the support have also been documented. However, the broken position of the strong and massive roof not only has a great impact on the stability of its below support and face but also influences the behaviors and movement of a few weaker roof layers sitting right above this hard roof. Therefore, more

research needs to be done regarding the characteristics of the gradual upward extension of the roof breakage, including the broken positions of different roof layers, rock broken angle α and strata broken angle φ , which are considered closely related to the geometric configurations of the disturbed overlying strata above the gob (see Fig. 3 for the definitions of these parameters). This study may help improving the ground control in the open face area, optimizing the face support design and predicting the surface subsidence. This paper therefore attempts to study the movement and broken positions of the overlying strata through a theoretical analysis and physical models.

Analytical solutions for the overburden movement

The broken positions of the roof strata and the consequent geometric caving configurations of the overlying strata above the face and the gob may have a major impact on the mine pressure behaviors in the open face area. The roof broken position, on the other hand, is affected not only by its thickness, strength, and stiffness, but also the loading characteristics of the upper rock layers and the deformation or stiffness of the lower strata. It is necessary to understand how these influencing factors affect the caving characteristics of the strong and hard roof as well as the upper few weaker roof layers.

Development of a roof failure analytical model

The immediate roof caves in upon the advance of the roof supports and the fresh main roof overhangs. The strong and hard main roof breaks when the limit broken length of the cantilever roof beam is reached. In this paper, an analytical model combining the beam on the elastic foundation theory

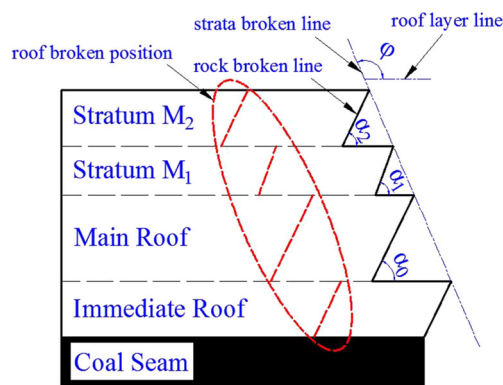


Fig. 3 A schematic for the definitions of the rock broken angle α , strata broken angle φ , and roof broken position. Rock broken angle α is defined as the angle between the rock broken line and the roof layer line, strata broken angle φ is defined as the angle between the strata broken line and the roof layer line

and the cantilever beam theory is proposed for analyzing the broken positions of the roof strata above the face and the consequent geometric configurations of the overburden behind the support after caving. Figure 4 gives a schematic of the analytical model, in which b and l are the length of beams OA and AB, respectively; h is the thickness of the main roof; origin of coordinates is set at point O with the horizontal X coordinate pointing to the gob direction and vertical Y-coordinate pointing downward. In this model, the main roof OB has two segments, i.e., beam OA sitting on the elastic foundation (say the immediate roof and the coal seam) and the cantilever beam AB overhanging behind the face. Note that point O is assumed far beyond the influencing area of the front abutment pressure. Rotation and moment at point O are therefore 0. On the other hand, the cantilever beam AB is fixed at point A. We assume that the maximum moment M_A and shear force Q_A are found at point A (see Fig. 4), and the rotation and displacement at this point are not 0. By contrast, the other side of the cantilever beam AB (point B) is assumed free. The overlying pressure on the main roof might be influential to the broken position of the roof. For simplification, a uniformly distributed pressure q is assumed in this paper for the overlying pressure on the main roof (beam OB).

The below coal seam and immediate roof are the elastic foundation supporting the main roof. In this paper, we define a supporting factor k_0 as the roof pressure on the foundation resulting in per unit vertical displacement of the foundation (Long 1982). By assuming that the total vertical displacement of the foundation is y , the force to the main roof provided by unit area of the foundation is $k_0 \times y$. Hence, the following equation can be obtained:

$$EIy^{(4)} = q - k_0y$$

where E is the elastic modulus, and I is the second moment of area of the beam.

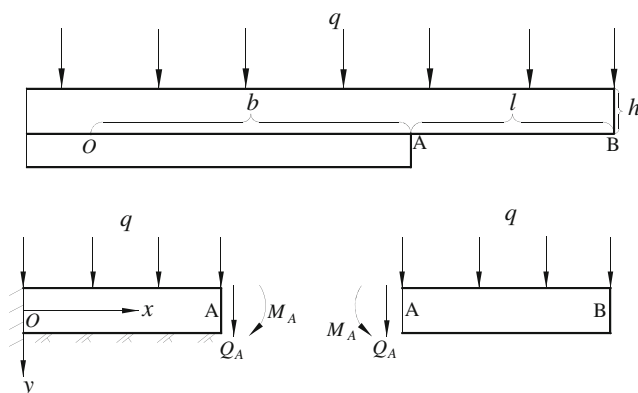


Fig. 4 The roof failure analytical model combining the beam on elastic foundation theory and the cantilever beam theory

By solving the above equation, we can have the following deflection equation of the beam OA on the elastic foundation, which is given as

$$y = y_0 \cdot \phi_1(\beta x) + \frac{\theta_0}{\beta} \phi_2(\beta x) - \frac{M_0}{EI\beta^2} \phi_3(\beta x) - \frac{Q_0}{EI\beta^3} \phi_4(\beta x) + \frac{q}{k} [1 - \phi_1(\beta x)]$$

where

$$\begin{aligned} \phi_1(\beta x) &= ch(\beta x)\cos(\beta x) \\ \phi_2(\beta x) &= (ch(\beta x)\sin(\beta x) + sh(\beta x)\cos(\beta x))/2 \\ \phi_3(\beta x) &= sh(\beta x)\sin(\beta x)/2 \\ \phi_4(\beta x) &= (ch(\beta x)\sin(\beta x) - sh(\beta x)\cos(\beta x))/4 \\ \beta &= \sqrt[4]{k/(4EI)} \end{aligned}$$

In the above equations, y_0 , θ_0 , Q_0 , and M_0 are the vertical displacement, rotation, shear force, and moment of the beam at point O. β is a feature coefficient in m^{-1} , a comprehensive parameter relative to the elastic performance of the beam (the main roof) and the foundation (the immediate roof and coal seam). This coefficient is influential to the stress and displacement of the main roof. k is a product of k_0 and the width of the beam (in the face width direction).

For a beam with a unit width, the feature coefficient can be described as

$$\beta = \sqrt[4]{3k_0/(Eh^3)}$$

Combining that $y_0 = 0$ and $\theta_0 = 0$ at point O, the equations for the deflection, rotation, moment, and shear force are given in Eqs. 1, 2, 3, and 4, respectively:

$$y = -\frac{M_0}{EI\beta^2} \phi_3(\beta x) - \frac{Q_0}{EI\beta^3} \phi_4(\beta x) + \frac{q}{k} [1 - \phi_1(\beta x)] \tag{1}$$

$$\theta = \frac{dy}{dx} = -\frac{M_0}{EI\beta} \phi_2(\beta x) - \frac{Q_0}{EI\beta^2} \phi_3(\beta x) + \frac{4\beta q}{k} \phi_4(\beta x) \tag{2}$$

$$M = -EI \frac{d\theta}{dx} = M_0 \cdot \phi_1(\beta x) + \frac{Q_0}{\beta} \phi_2(\beta x) - \frac{q}{\beta^2} \phi_3(\beta x) \tag{3}$$

$$Q = \frac{dM}{dx} = -4\beta M_0 \cdot \phi_4(\beta x) + Q_0 \cdot \phi_1(\beta x) - \frac{q}{\beta} \phi_2(\beta x) \tag{4}$$

Substituting the moment and shear force values at point A ($M = M_A$, $Q = Q_A$) into Eqs. 3 and 4 yields

$$Q_0 = \frac{1}{\phi_1^2 + 4\phi_2\phi_4} \left(\frac{\phi_1\phi_2 + 4\phi_3\phi_4}{\beta} q + \phi_1 Q_A + 4\beta\phi_4 M_A \right) \tag{5}$$

$$M_0 = -\frac{1}{\beta^2(\phi_1^2 + 4\phi_2\phi_4)} [(\phi_2^2 - \phi_1\phi_3)q + \beta\phi_2Q_A - \phi_1\beta^2M_A] \quad (6)$$

For the cantilever beam AB, we can easily get the moment and shear force values expressed as $Q_A = ql$ and $M_A = -ql^2/2$. Equations 5 and 6 are then changed as Eqs. 7 and 8 shown below:

$$Q_0 = \frac{q}{\phi_1^2 + 4\phi_2\phi_4} \left(\frac{\phi_1\phi_2 + 4\phi_3\phi_4}{\beta} + \phi_1l - 2\beta\phi_4l^2 \right) \quad (7)$$

$$M_0 = -\frac{q}{\phi_1^2 + 4\phi_2\phi_4} \left(\frac{\phi_2^2 - \phi_1\phi_3}{\beta^2} + \frac{\phi_2l}{\beta} + \frac{1}{2}\phi_1l^2 \right) \quad (8)$$

where $\phi_n = \phi_n(\beta b)$, $n = 1, 2, 3$, and 4.

Combining the above equations, we can have the deflection, rotation, moment, and shear force at any position in the beam OB.

Based on the proposed analytical model, we can determine the roof broken position, strata broken angle, and consequently the caving geometric characteristics of the overlying strata.

Determination of the roof broken positions

The breakage of the main roof might be a result of both the weight of the above overlying strata and the upward pressure provided by the below strata. Therefore, this paper considers both the overburden pressure q and supporting factor k_0 in the proposed analytical model. Note that the roof typically fails in tension and the broken position of the roof occurs at the maximum moment (and 0 for shear force at this position). Since the shear force at point A is not 0, the moment at this position is therefore not the maximum value. The main roof therefore breaks ahead of point A. With the advance of the longwall face, the main roof overhangs behind the face, and the mined-out void in the open face area allows the displacement and rotation of the main roof. The above strata, however, have less available space or separation for displacement due to the support of the main roof, shields, and the gob materials. Therefore, the main roof and the overlying strata may present different broken positions. This is analyzed below separately.

Broken position of the main roof

The main roof breaks at the position where the shear force is 0 and the bending moment reaches its maximum. The calculation of the roof broken position requires combining Eqs. 3, 4, 7, and 8. A parametric study is performed by substituting typical parameters into the expression for the broken position of the main roof. Since the closed-form solution for the roof broken position is way too complex, this paper only gives the results calculated from a MATLAB code.

It is not unreasonable to assume that $E = 30$ GPa, $\sigma_t = 3.5$ MPa, $q = 0.5$ MPa, and $k = 0.5\text{--}2$ GPa, where E is the

modulus of the main roof, σ_t is the tensile strength, q is the uniformly distributed pressure on the main roof, k is the supporting factor, and the suggested values can be found from Long (Long 1982). Table 1 gives the results obtained from a MATLAB code.

In Table 1, h represents the thickness of the strong roof above the seam. It is learned that the broken position ahead of the longwall face increases with the thickness of the roof but decreases with the increase of supporting factor. A thin main roof with a low supporting factor breaks at a smaller distance ahead of the immediate roof line. For example, the broken position of a 5-m main roof with a supporting factor of 0.5 occurs at 3.38 m ahead of the immediate roof. In western mining areas of China (the 4 major coal bases) where the thin bedrock is commonly found, the broken position of the main roof falls in the range of the shield's supporting area, which might result in a dynamic load on the shields when the roof breaks. Field observation confirms this mine pressure behavior that a tremendous working resistance is commonly found on the legs of the shields during periodic roof weightings. Hence, this finding of the analytical model should be helpful for predicting the dynamic mine hazards during weighting and improving the performance of the face and shields.

Broken positions of the strata above the main roof

The breakage of the main roof creates separation and space for the movement of the very above weaker stratum, say Stratum M_1 in Fig. 5a. Assuming the roof beams have the same limit broken length ($L_0 = L_1$), the overhang length of Stratum M_1 can be expressed as

$$l_1 = L_1 - z_1 = (l_0 + z_0) - z_1$$

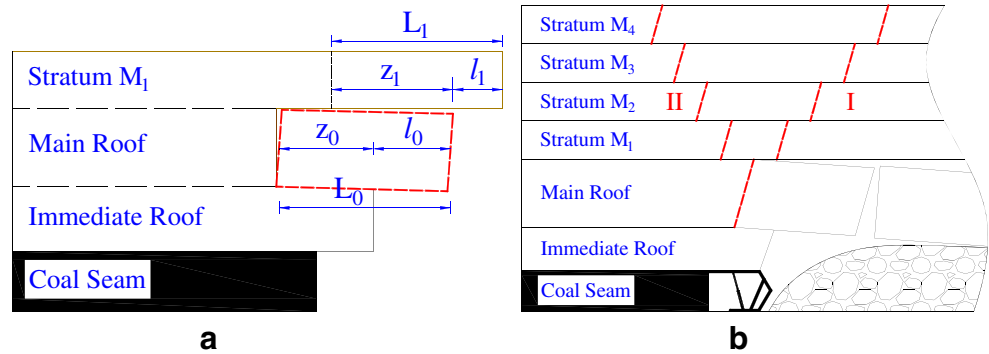
where l_0 and l_1 are the overhang lengths of the main roof and Stratum M_1 , z_0 , and z_1 are the distance ahead of the lower roof line for the main roof and Stratum M_1 . L_0 and L_1 are the limit broken lengths of the main roof and Stratum M_1 .

Depending on the relative magnitude of l_1 and L_1 , the broken positions of above strata can be divided into two modes. If the unsupported overhang length of the Stratum M_1 is larger than its limit broken length ($l_1 > L_1$), Stratum M_1 and its overlying strata would fail as Mode I shown in Fig. 5b. During the periodic breaks of the main roof, it is observed that the

Table 1 Broken positions of the main roof ahead of the immediate roof line under different geologic conditions

h/m	k/(GPa·m ⁻¹)			
	0.5	1.0	1.5	2.0
5	3.38	2.58	2.20	1.96
10	5.16	3.91	3.31	2.94
15	6.58	4.97	4.20	3.72
20	7.82	5.88	4.97	4.40

Fig. 5 Two modes of the broken positions of the main roof and the above weaker strata



released unsupported area of the above Stratum M_1 is not increasing progressively but at an interval. The maximum bending moment at the broken position is larger than its ultimate bending moment. Therefore, the position where the bending moment reaches the maximum value indicates the roof broken position. In this case, Stratum M_1 has the same broken length with the main roof.

If the limit broken length of Stratum M_1 is larger than the overhang length ($L_1 > l_1$), Stratum M_1 may maintain its stability since the main roof provides support for Stratum M_1 . When the main roof breaks again, the unsupported overhang length of Stratum M_1 increases suddenly and dramatically. By this time, the overhang length is typically larger than its limit broken length. Stratum M_1 breaks as Mode II. Likewise, the broken position occurs at the maximum bending moment. During the calculation, the overhang length of Stratum M_1 (l_1) is assumed to be twice the limit broken length of the main roof ($2L_0$). Considering that the shear force is 0, the position where bending moment reaches the maximum, i.e., the roof broken position. In this case, the broken length of Stratum M_1 is twice the main roof. The strata above Stratum M_1 have the similar broken positions.

The broken positions of the overlying strata above the main roof depend on the maximum bending moment rather than the tensile strength of the strata. The overhang length of the strata in Mode II is twice that Mode I; therefore, the roof broken positions ahead of the longwall face are different.

Parametric analysis on the broken positions of the overlying strata

The shear force should be 0 at the positions where the roof break. Let $z = b - x$ and combine Eqs. 4, 7, and 8; we can have the expression for the distance of the i_{th} stratum ahead of its lower $(i-1)_{th}$ stratum, i.e., z_i . Note that x is the distance from the front side of the beam (see Fig. 4 the coordinate system), and b is the length of the beam sitting on elastic foundation (for instance, the length of beam OA for the main roof in Fig. 4). It is better choosing a large value of b . The front side of the beam therefore stays far beyond the abutment pressure influencing area.

The following steps give the method for calculating the broken positions of the overlying strata.

1. By assuming $b = 2m\pi$, where m is a large positive integer, we can have $ch(\beta b) = sh(\beta b) = e^{2m\pi\beta}/2$.
2. Substituting the above equation into Eqs. 7 and 8 yields the expressions for Q_0 and M_0 .
3. Substitute the obtained expressions for Q_0 and M_0 into Eq. 4, and let Eq. 4 equal 0; the formula for z_i can be obtained and given below in Eq. 9. Note that during the calculation, the expression $z = b - x$ is changed back to $x = b - z$:

$$z_i = \frac{1}{\beta_i} \arctan \frac{1}{\beta_i l_i + 1} \text{ and } z_i + l_i = L_0 \tag{9}$$

where β_i is the feature coefficient of the elastic foundation for the i_{th} stratum. l_i is the overhang length of the stratum ($l_i > L_i$). L_0 is the broken length of the main roof.

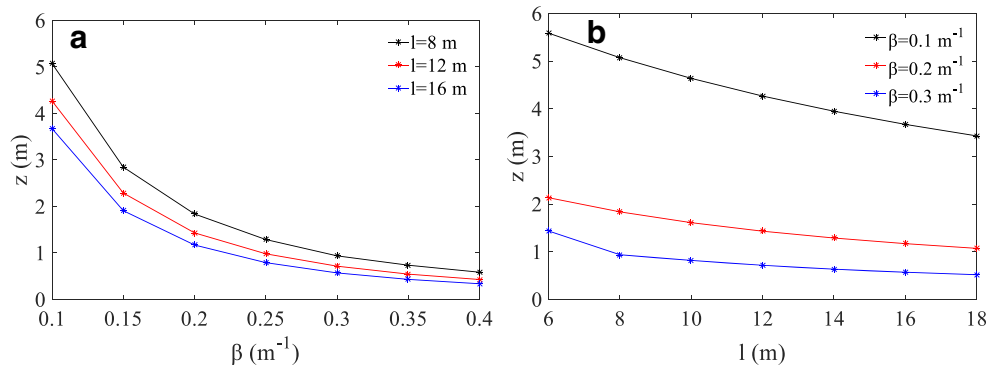
Figure 6 gives the relationship between the length of the roof ahead of its very below roof line (z) and the feature coefficient (β) and the overhang length (l). It shows that z decreases with increasing β and l . Note that a small value of z means that the broken position is closer to the faceline/power support.

Analysis on the caving characteristics of the overlying strata

Geometric configurations of the caving overburden

The geometric configuration of the overlying strata above the gob is influenced by both the roof broken positions and strata broken angle. Theoretically, the configurations can be classified into three types, the trapezoid-shaped, rectangular-shaped, and inverted trapezoid-shaped configurations given in Fig. 7. Figure 7a plots the regular trapezoid-shaped configuration, in which the strata broken angle φ is less than 90° . This is because the length of the roof ahead of the lower roof

Fig. 6 The relationships between **a** roof broken length ahead of the lower stratum and the feature coefficient at different overhang lengths; **b** roof broken length ahead of the lower stratum and the overhang length at different feature coefficients



line (z_i) is less than half of the roof overhang length ($0.5h_i \times \tan\theta_i$), or $z_i < 0.5h_i \times \tan\theta_i$. The rectangular-shaped configuration is given in Fig. 7b where $\varphi = 90^\circ$. In this case, $z_i = 0.5h_i \times \tan\theta_i = 0$. Figure 7c shows the inverted trapezoid-shaped configuration where $\varphi > 90^\circ$ and $z_i > 0.5h_i \times \tan\theta_i$.

Rock broken angle

The caving configurations of the disturbed overlying strata above the gob are influenced by not only the breaking positions of the strata, but also the rock broken angle and the strata broken angle. Based on the field observation, the rock broken angle is slightly less than 90° (see α in Fig. 8) and the roof block rotates after its breakage (see θ in Fig. 8). The relationship of the roof block rotation angle and the rock broken angle is given as $\alpha = 90^\circ - \theta$.

Substituting the coordinate values at the roof broken position into Eq. 2 gives the expression for the roof block rotation angle θ shown in Eq. 10:

$$\theta = \frac{ql \cdot \sqrt{\beta^2 l^2 + 2\beta l + 2}}{2EI\beta^2} \cdot e^{-\arctan\frac{l}{\beta l + 1}} \tag{10}$$

where θ is the roof block rotation angle in *rad*.

It can be seen from Eq. 10 that θ has a positive relationship with q/EI and is also related to the feature

coefficient β and the overhang length of the roof l . Figure 9 shows the variation of the roof block rotation angle over the feature coefficient and the overhang length of the roof. It should be noted that the Y-coordinate is $EI\theta/q$, a dimensionless parameter that can be used to describe the rotation of the roof block when EI/q is determined in a certain condition. It shows that θ decreases with the increase of β and increases with the increase of l (or equivalently, α increases with the increase of β and decreases with the increase of l).

Strata broken angle

Assuming in a coal mine a 6.75-m thick Stratum 1 overhangs 14.7 m after the breakage of the main roof, the Stratum 1 applies a vertical pressure of 0.206 MPa to the main roof, and the elastic modulus, tensile strength, and supporting factor are 11 GPa, 1.5 MPa, and 1.0 GN/m³, respectively. Substituting these figures into Eq. 9 yields $z_1 = 1.6$ m and $\theta_1 = 0.03^\circ$. Therefore, the block rotation angle θ is negligible and consequently, the rock broken angle α is close to 90° . Field observation also confirms that the roof block rotation angle θ is small in the field. On the other hand, the inverted trapezoid-shaped configuration is mostly observed. As a result, the configuration given in Fig. 7c is re-plotted as Fig. 10 with the strata broken angle φ larger than 90° , and the rock broken angle α equal to 90° .

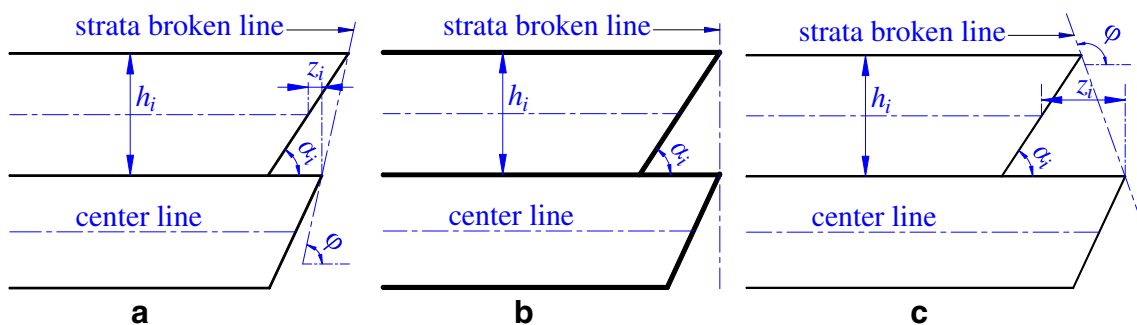


Fig. 7 **a** Regular trapezoid-shaped configuration. **b** Rectangular-shaped configuration. **c** Inverted trapezoid-shaped configuration

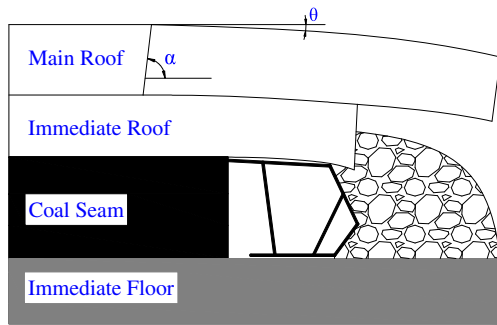


Fig. 8 Roof block rotation angle θ and rock broken angle α

The strata broken angle φ can be given as

$$\varphi = \frac{\pi}{2} + \arctan \frac{z}{h} = \frac{\pi}{2} + \arctan \left(\left(\frac{3k_0}{E} \right)^{-0.25} h^{-0.25} \arctan \frac{1}{lh^{-0.75} \left(\frac{3k_0}{E} \right)^{0.25} + 1} \right) \quad (11)$$

From Eq. 11, it is found that the strata broken angle φ increases with the decrease of k_0/E and l . The thickness of the roof layer h also has an impact on the strata broken angle, but this impact varies under different conditions. Assuming that $E = 30$ GPa, $k_0 = 0.3$ GN/m³, and $l = 11.62$ m, Fig. 11a shows that φ increases with h . While if the overhang length decreases to $l = 5$ m, φ first increases then decreases with the increase of h (see Fig. 11b). In both figures, however, φ is larger than 90° , indicating an inverted trapezoid-shaped configuration of the caving overlying strata above the gob.

A case study

This paper gives a case study for the application of the proposed model. The necessary parameters of the studied coal mine are listed in Table 2. Equation 12 is first used to calculate the pressure on each stratum to determine the strong and hard key stratum (Qian 1983). The results show that Stratum 5 is the key stratum:

Fig. 9 The relationships between **a** the roof block rotation angle and feature coefficient under different overhang lengths and **b** the roof block rotation angle and overhang length under different feature coefficients

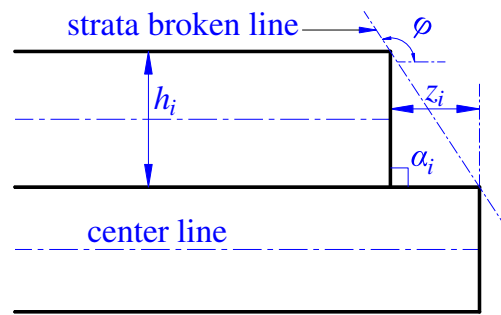
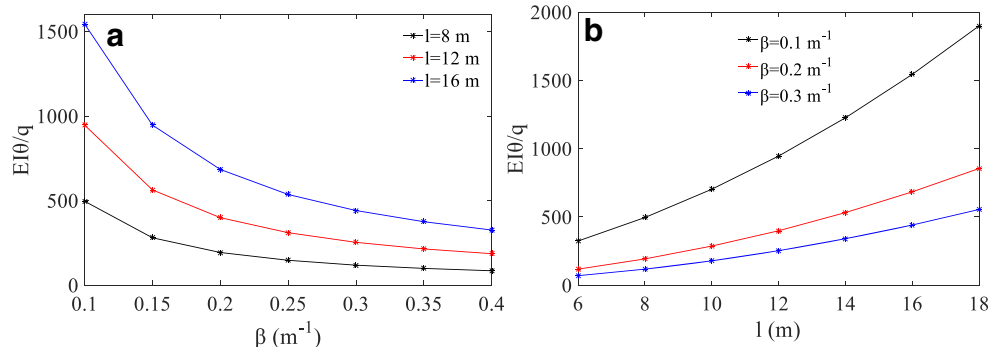


Fig. 10 The inverted trapezoid-shaped configuration with a 90° of rock broken angle

$$(q_n)_1 = \frac{E_1 h_1^3 (\gamma_1 h_1 + \gamma_2 h_2 + \dots + \gamma_n h_n)}{E_1 h_1^3 + E_2 h_2^3 + \dots + E_n h_n^3} \quad (12)$$

where E_i is the elastic modulus of each stratum ($i = 1, 2, \dots, n$). h is the thickness of each stratum. γ is the unit weight.

The following Eq. 13 is then used to estimate the limit broken length of each beam (Qian 1983). It shows that the largest limit broken length occurs at the main roof instead of the above roof strata. Therefore, the failure mode of the roof in this case can be determined as Mode I (see Fig. 5b):

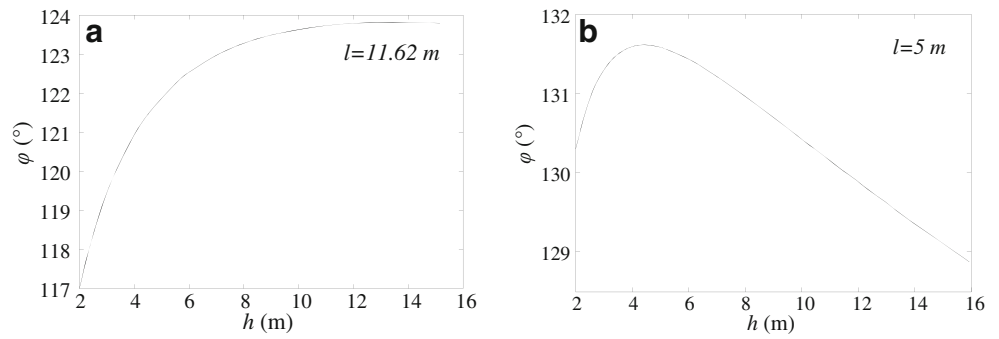
$$L = h \sqrt{\frac{\sigma_t}{3q}} \quad (13)$$

where L is the limit broken length of the beam; h is the strata thickness, σ_t is the tensile strength, and q is the uniform distributed load.

The interval of the main roof failure can be obtained based on Eq. 8 using a MATLAB code. The broken position and broken angle can be determined by combining Eqs. 9, 10, and 11. The results are given in Table 3 and Fig. 12. It shows that the strata broken angle φ is 110° , which is in good agreement with the field measurement.

The theoretical analysis reveals that the strata broken angle (φ) changes under different geological and mining conditions. If $\varphi < 90^\circ$, the final configuration of the roof after break is trapezoid-shaped; $\varphi = 90^\circ$ and $\varphi > 90^\circ$ yield the rectangular and inverted trapezoid-shaped configurations, respectively. Of

Fig. 11 The variation of the strata broken angle over thickness of the roof strata



those, the inverted trapezoid-shaped configuration is mostly observed in the field.

Physical modeling study

The conventional physical model only reproduces the trapezoid-shaped configuration in the previous physical modeling studies. This might be due to the unrealistic governing parameters in the physical modeling. These investigations have developed an improved physical modeling rig to reproduce three of the overlying configurations predicted by the theoretical model. The deviation analysis on the previous physical modeling studies is first presented to determine the governing parameters according to the proposed theoretical model.

Deviation analysis on conventional physical modeling studies

Physical modeling is commonly used in the laboratory for studying the roof strata movement above a longwall face. Figure 13 gives a typical geometric configuration of the roof strata after caving at the final advance of face. It shows a regular trapezoid-shaped caving configuration. However, the strata geometric configuration after caving might be different in the field under different geological and mining conditions. For instance, in the thin-bedrock longwall faces at four of the abovementioned coal bases, a

large-scale vertical crack developed from the faceline up to the surface is frequently observed (rectangular-shaped configuration, $\varphi = 90^\circ$). The inrush of water or sand into the open face area along the large-scale crack may occur. The breakage of the hard roof along the faceline may generate dynamic load on the roof supports, leading to the poor performance or failure of the supports.

The conventional physical models are not capable of accurately capturing the roof broken position, strata broken angle, and the interaction between the roof and supports. This might be due in part to the inapplicable governing parameters such as the feature coefficient (β), the ratio of the uniformly distributed load over roof stiffness (q/EI), the ratio of tensile strength over the uniformly distributed load (σ_t/q), and the dimensionality of the model, which is illustrated below in detail.

The feature coefficient β ($\beta = (k/4EI)^{0.25}$)

The feature coefficient β might be the most important parameter that affects the roof broken position and strata broken angle, which is widely ignored in the conventional physical models. Generally, the feature coefficient β in the conventional physical models is larger than that in the field. It is found that the feature coefficient of the roof materials in the physical model is about 20, compared to approximately 0.2 in the field. Therefore, the upper roof breaks behind or along the lower roof line in the physical model, resulting in the trapezoid-shaped caving configuration. To realistically simulate the roof movement, the

Table 2 Mechanical properties of overlying strata

Strata	Lithology	γ , MN/m ³	h , m	E , GPa	k_0 , 10 ⁹ N/m ³
Stratum 5	Mudstone	0.024	15.15	11	0.3–0.4
Stratum 4	Fine-grained sandstone	0.025	4.05	30	0.8–1.2
Stratum 3	Mudstone	0.024	7.8	11	0.3–0.4
Stratum 2	Medium-grained sandstone	0.025	2.4	27	0.4–0.6
Stratum 1	Mudstone	0.025	6.75	11	0.3–0.4
Main roof	Fine-grained sandstone	0.025	8.75	30	0.8–1.2

Table 3 A list of the calculation results

Strata	k_0 , GPa/m	σ_t , MPa	q, MPa	β	s' , m	s/m	α , °	z, m	φ , °
Stratum 4	0.35	3.5	0.101	0.152	13.76	$L0 = 10 + z0 = 12.3 + 4.0 = 16.3$	89.97	2	116.5
Stratum 3	0.5	1.5	0.209	0.13	12.06		89.98	2.7	108.8
Stratum 2	0.35	3	0.06	0.23	9.8		89.94	0.9	111.4
Stratum 1	1	1.5	0.206	0.173	10.52		89.97	1.6	103.3
Main roof	0.75	3.5	0.46	0.103	13.93		89.99	4	114.8

L' is the estimated limit broken length of the overlying roof beam. L is the limit broken length of the main roof. In the case where the elastic foundation has two layers, e.g., the upper laminated layer and the lower massive one, the supporting factor of the foundation can be calculated by using $k_0 = E_0/H$, where H is the foundation thickness and E_0 is the foundation modulus. For instance, when the main roof is the beam on elastic foundation, the upper foundation is the laminated immediate roof and coal seam, while the lower foundation is the massive floor. The supporting factor is given as $k_0 = 0.75$ GPa/m, where the average modulus of the foundation is 3 GPa and the seam thickness is 4 m

feature coefficient should be decreased. This can be achieved by increasing the elastic modulus of the roof materials or reducing the supporting coefficient.

The ratio of the uniformly distributed load over roof stiffness (q/EI)

The strata broken angle is not only affected by the feature coefficient but also the ratio of the uniformly distributed load over the roof stiffness (q/EI). Note that the roof load on the coal seam is assumed as the uniformly distributed load in this paper. The broken angle trends to be proportional to q/EI , or equivalently $\rho/(Eh^2)$, in which is ρ the density of the construction material in the physical model. In the conventional physical models, this ratio is 10^7 times the in situ value. As a result, the broken angle obtained in the physical model is unrealistically larger than that observed in the field. To solve this problem, we need to select physical materials with small density and large modulus and improve the overall size of the physical model.

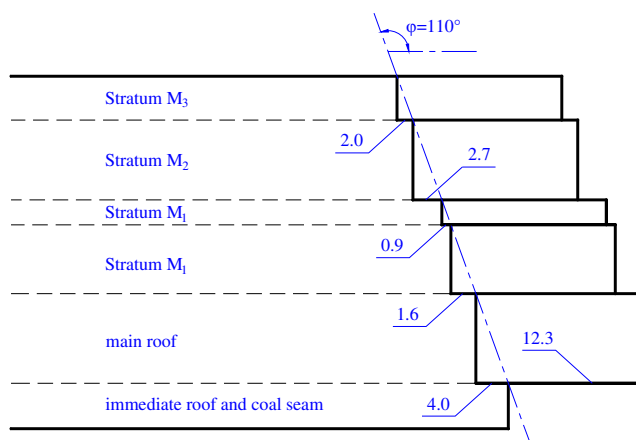


Fig. 12 The roof broken position and the strata broken angle of the studied coal mine

The ratio of tensile strength over the uniformly distributed load (σ_t/q)

The compression strength ratio is one of the three major similarity ratios that a conventional physical model must follow. However, the roof both in the physical model and the field fail in tension. Tensile strength of the roof rocks is therefore a more important parameter than the compression strength for a physically realistic simulation. Tensile strength of the rock may change the extension length of the cantilever roof beam, and consequently, the caving configuration of the overlying roof strata. Generally, a larger tensile strength leads to a longer overhang length of the cantilever roof beam. Hence, care should be taken to ensure proper density for the physical materials and a proper tensile strength ratio for the physical model.

The dimensionality of the model

Generally, the conventional 2D physical model is less than 20 cm wide (the face width is less than 20 cm). The length of the model is also too small to achieve a critical extraction.

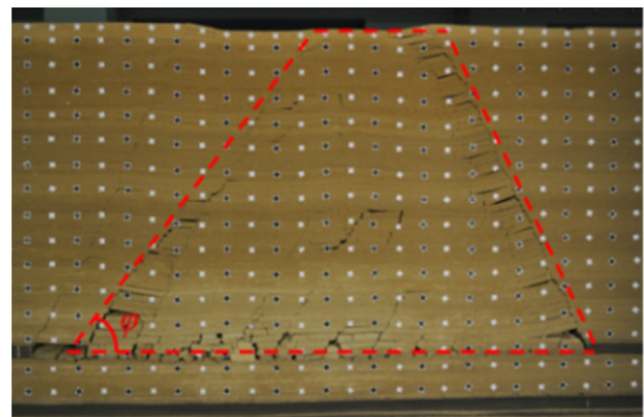


Fig. 13 The typical regular trapezoid-shaped roof caving configuration captured in the conventional physical model at final face advance. The strata broken angle φ is less than 90°

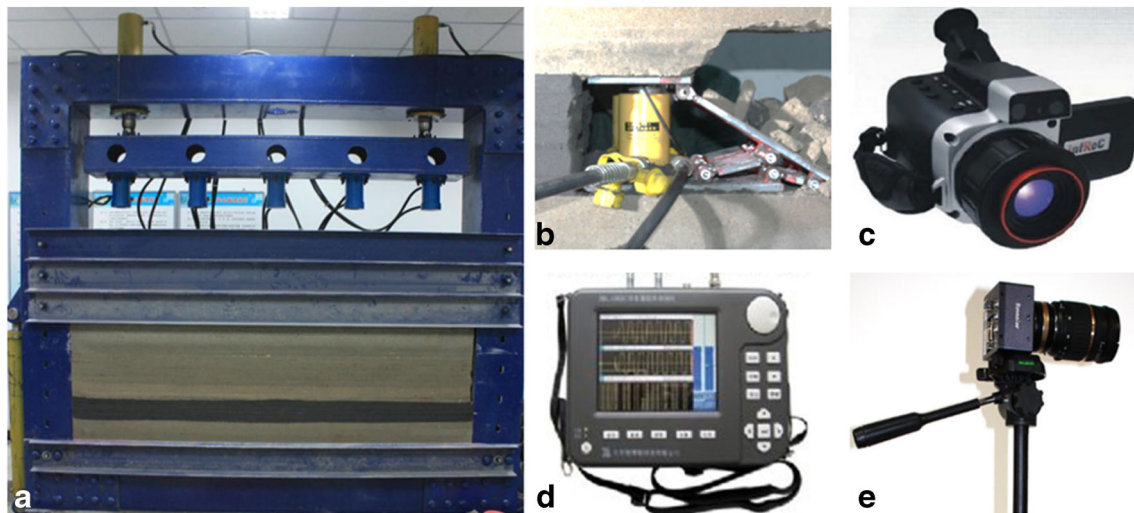


Fig. 14 Final construction of the physical model and the measuring system. **a** Physical modeling rig. **b** Load sensor installed on the support. **c** Infrared imaging system. **d** Ultrasonic detection system. **e** High-speed imaging system

By increasing the overall size of the physical modeling rig, the similarity ratio is increased with an enlarged mining area, and the impact of the model boundaries is reduced with improved accuracy.

Development of an improved physical model

Based on the above deviation analysis, the biomechanical properties of the physical model for different strata are the most important factor affecting the experimental accuracy. Therefore, the construction materials should be chosen carefully at the first place and the biomechanical properties of the roof layers should be determined by adjusting the proportions of the construction materials through a trial-and-error procedure. Thus, the abovementioned governing factors can be kept as close to those in the field as possible. During the physical modeling test, movement of the roof strata (including the creation of the mining induced cracks) is only produced due to the mining activities.

Secondly, the overall dimension of the test rig should be increased. Figure 14 shows the improved physical modeling

rig developed by the principal author of this paper. The $3000 \times 500 \times 4000$ -mm modeling rig is significantly larger than the conventional one with a typical width of 200 mm. A total of five hydraulic rams are evenly displaced on the top of the model to simulate the overall weight of the overburden that cannot be constructed in the physical model. The hydraulic cylinder provides a maximum stroke of 1000 mm and maximum load of 50 t. The test rig enables modeling of an enlarged mining area with increased similarity ratio and reduced boundary effect.

The measuring system is also an important part of the physical modeling. This experiment includes displacement measuring system, strain measuring system, ultrasonic detection system, infrared imaging system, and high-speed imaging system for gathering the necessary data on the roof movement during the face advance. A load sensor (type SZY-3-B) is used for monitoring the changes of the support's working resistance with face advance for studying the interaction between the roof and support. The sensor is able to capture 100 load data per second. Note that this paper mainly concerns the configuration of the overburden induced by the longwall mining; the displacement and stress data are therefore not included.

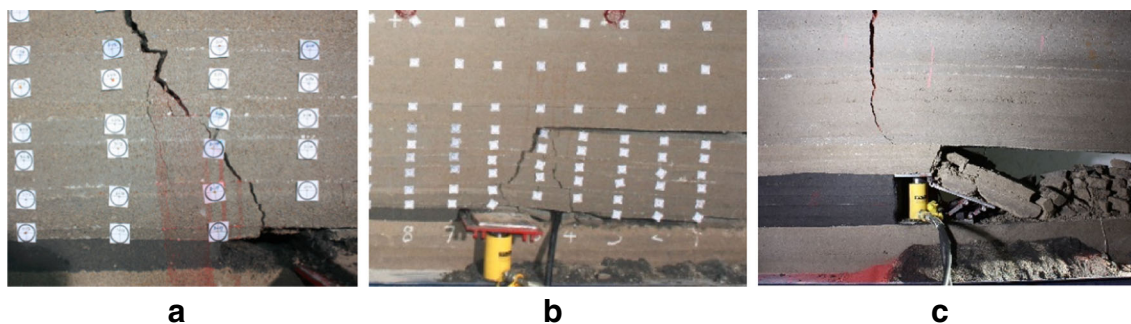


Fig. 15 Geometric configurations of the caving strata under different experimental conditions. **a** Reversed trapezoid roof caving configuration. **b** Regular trapezoid roof caving configuration. **c** Rectangular roof caving configuration

Results and analysis

The improved physical modeling rig is used to reproduce the caving configurations of the strata after mining. Figure 15 gives the geometric configurations of the caving strata under different experimental conditions. A massive strong roof layer produces a reversed trapezoid-shaped configuration, in which the broken position of each roof layer extends upward ahead of the face ($\varphi > 90^\circ$; see Fig. 15a). The soft roof, however, creates a trapezoid-shaped caving configuration, in which the roof broken position extends upward behind the face ($\varphi < 90^\circ$; see Fig. 15b). The thin-bedrock roof produces a rectangle-shaped caving configuration, in which the crack develops upward vertically ($\varphi = 90^\circ$; see Fig. 15c). These configurations (especially the reversed trapezoid-shaped and the rectangle-shaped one) are not commonly found in the previous conventional physical modeling. The physical modeling properly reproduces the three caving configuration of the strata above the gob, which can be used to validate the proposed theoretical model.

Summary and conclusions

The broken positions of the roof may have an impact on the geometric configurations of the caving strata and the mine pressure behaviors in the open face area. This paper has developed an analytical model combining the cantilever beam theory and beam on elastic foundation theory to obtain the roof broken positions, rock broken angle, and strata broken angle, which can be used for describing the caving configurations of the disturbed strata above the gob. The proposed analytical model yields three different caving configurations including the regular trapezoid-shaped, rectangular-shaped, and inverted trapezoid-shaped configurations. A case study is also provided to illustrate the application of the analytical model. The proposed roof failure analytical model gives the closed-form solutions for the roof broken position (z), rock broken angle (α), and the strata broken angle (φ), according to which the geometric caving configuration of the overlying strata can be classified as the regular trapezoid-shaped, rectangular-shaped, and inverted trapezoid-shaped. The roof broken position (z) and the rock broken angle (α) are largely influenced by both the feature coefficient (β), overhang length (l) of the roof beam, and the tensile strength of the roof. The roof broken position (z) has a negative relationship with the feature coefficient (β) and the overhang length (l), while the rock broken angle (α) has a positive relationship with the feature coefficient (β) and negative relationship with the overhang length (l). The strata broken angle is typically larger than 90° , indicating an inverted trapezoid-shaped configuration.

The conventional physical models can only reproduce the regular trapezoid-shaped configuration due to the inapplicable

governing parameters. These parameters may influence the roof caving characteristics and are identified through a deviation analysis. An improved physical modeling rig is therefore developed based on the deviation analysis to reproduce the movement of the roof strata in a physically realistic way. The prerequisite is that the construction materials of the physical model should be chosen carefully to develop proper physical rock layers with reasonable biomechanical properties and that the stress and displacement boundary conditions should be met. The improved physical rig realistically reproduces the regular trapezoid-shaped, the rectangular-shaped, and the inverted trapezoid-shaped configurations predicted by the theoretical model. Future studies will consider observations of acoustic emission events and ultrasonic velocity in the physical models, and monitoring of microseismic in the field for predicting the broken positions of the roof strata ahead of longwall face.

Funding information This research was supported by the National Key Research and Development Project [2017YFC0603002], National Natural Science Foundation of China [51974320], and Beijing Natural Science Foundation [2204080].

References

- BP (2017) BP Statistical Review of World Energy. British Petroleum
- Fan LM, Ma XD, Jiang H et al (2016) Risk evaluation on water and sand inrush in ecologically fragile coal mine. *J China Coal Soc* 41(3): 531–536 (in Chinese)
- Gao ZG (2012) Sustainable development and upgrading mode of coal industry in China. *Int J Min Sci Technol* 22:335–340
- Ghose AK (2003) Why longwall in India has not succeeded as in other developing countries like China. *Int J Min Sci Technol* 84:1–4
- Han HJ, Zeng MS, Song ZY et al (2017) Research on key technology of powered support design in 8.2 m large mining height face. *Coal Sci Technol* 45(11):63–68 (in Chinese)
- Huang QX, Qian MG, Shi PW (1999) Structural analysis of main roof stability during periodic weighting in longwall face. *J China Coal Soc* 24(6):581–585 (in Chinese)
- Jia XR, Huo YD (1999) The review of ground pressure theory of thin slab in coal mining and its application. *J Min Saf Eng* 3:22–25 (in Chinese)
- Li XY, Ma NJ, Zhong YP et al (2007) Storage and release regularity of elastic energy distribution in tight roof fracturing. *Chin J Rock Mech Eng* 26(sup. 1):2786–2793 (in Chinese)
- Li N, Wang EY, Ge MC et al (2015) The fracture mechanism and acoustic emission analysis of hard roof: a physical modeling study. *Arab J Geosci* 8(4):1895–1902
- Liu XJ, Luan HB (2015) A brief analysis of the circumstances of the current coal industry and its trends in China. *Int J Min Miner Eng* 6(1):87–96
- Long YQ (1982) Calculation of elastic foundation beam. People's Education Press, Beijing, pp 54–64 (in Chinese)
- Meng XR, Wu HT, Wang GB (2014) Development and method selection of thick coal seam mining technology in China. *Coal Eng* 46(10): 43–47
- Mondal D, Roy PNS, Behera PK (2017) Use of correlation fractal dimension signatures for understanding the overlying strata dynamics in longwall coal mines. *Int J Rock Mech Min Sci* 91:210–221

- National Energy Administration (2016) 13th FYP development plan for renewable energy. (in Chinese)
- Pan Y, Gu SD (2014) Analysis of bending moment, shear force, deflection and strain energy of hard roof at initial stage of cracking during periodic pressures. *Chin J Rock Mech Eng* 33(6):1123–1134 (in Chinese)
- Pan Y, Wang ZQ, Li AW (2012a) Analytic solutions of deflection, bending moment and energy change of tight roof of advanced working surface during initial fracturing. *Chin J Rock Mech Eng* 31(1):32–41 (in Chinese)
- Pan Y, Gu SD, Qi YS (2012b) Analytic solutions of tight roof's bending moment and deflection under swelling distributive supporting pressure. *Chin J Rock Mech Eng* 31(10):2053–2063 (in Chinese)
- Pan Y, Gu SD, Qi YS (2013) Analytic solution of tight roof's bending moment, deflection and shear force under advanced supercharger load and supporting resistance before first weight. *Chin J Rock Mech Eng* 32(8):1544–1553 (in Chinese)
- PENG SS, CHIANG HS (1984) Longwall mining. Wiley, New York, p 708
- Qian MG (1981) Conditions required for equilibrium of overlying strata at working areas. *J China Univ Min Techn* 2:34–43
- Qian MG (1983) Mining pressure and strata control. China Coal Industry Press, Beijing (in Chinese)
- Qian MG, Li HC (1982) The movement of overlying strata in longwall mining and its effect on ground pressure. *J China Coal Soc* 2:3–14 (in Chinese)
- Qian MG, Miao XX, Xu JL (1996) Theoretical study of key stratum in ground control. *J China Coal Soc* 21(3):225–230 (in Chinese)
- Qian MG, Xu JL, Wang JC (2018) Further on the sustainable mining of coal. *J China Coal Soc* 43(1):1–13 (in Chinese)
- Research Group of National Key Basic Research Program of China (2017) Theory and method research of geological disaster prevention on high-intensity coal exploitation in the west areas. *J China Coal Soc* 42(2):267–275 (in Chinese)
- Roy PNS, Sawmliana C, Bhagat NK (2003) Induced caving by blasting: innovative experiments in blasting gallery panels of underground coal mines of India. *Min Technol* 112(1):57–63
- Song GF, Chugh Y (2018) 3D analysis of longwall face stability in thick coal seams. *J South Afr Inst Min Metall* 118(2):131–142
- Song GF, Yang SL (2015) Investigation into strata behaviour and fractured zone height in a high-seam longwall coal mine. *J South Afr Inst Min Metall* 115(8):781–788
- Song GF, Pan WD, Yang JH et al (2015) Mining methods selection in thick coal seam based on fuzzy analytic hierarchy process. *J Min Saf Eng* 32(1):35–41
- Song GF, Chugh Y, Wang JC (2017) A numerical modeling study of longwall face stability in mining thick coal seams in China. *Int J Min Miner Eng* 8(1):35–55
- Verma AK, Deb D (2007) Analysis of chock shield pressure using finite element method and face stability index. *Min Technol Trans Inst Min Metall Sect A* 116(2):67–78
- Verma AK, Deb D (2010) Longwall face stability index for estimation of chock-shield pressure and face convergence. *Geotech Geol Eng* 28(4):431–445
- Wang JC (2009) Theory and technology of thick seam mining. Metallurgical Industry Press, Beijing (in Chinese)
- Wang GF, Pang YH (2015) Relationship between hydraulic support and surrounding rock coupling and its application. *J China Coal Soc* 40(1):30–34
- Wang GF, Pang YH (2016) Shield-roof adaptability evaluation method based on coupling of parameters between shield and roof strata. *J China Coal Soc* 41(6):1348–1353
- Wang GF, Pang YH (2018) Full-mechanized coal mining and caving mining method evaluation and key technology for thick coal seams. *J China Coal Soc* 43(1):33–42 (in Chinese)
- Wang JC, Wang ZH (2015) Stability of main roof structure during the first weighting in shallow high-intensity mining face with thin bedrock. *J Min Saf Eng* 32(2):175–181 (in Chinese)
- Wang JC, Zhong SH (2008) The present status and the key issues to be resolved of thick seam mining technique in China. *Sciencepaper Online* 3(11):829–834
- Wang JC, Yang SL, Li Y et al (2014) A dynamic method to determine the supports capacity in long wall coal mining. *Int J Min Reclam Environ* 1(1):1–14
- Wang JC, Liu F, Wang L (2016a) Sustainable coal mining and mining sciences. *J China Coal Soc* 41(11):2651–2660 (in Chinese)
- Wang GF, Pang YH, Zhang CC et al (2016b) Intelligent longwall mining technology and equipment and adaptability in super large mining height working face. *Coal Eng* 48(9):6–10 (in Chinese)
- Wang GF, Li XY, Zhang CC et al (2017a) Research and development and application of set equipment of 8 m large mining height fully-mechanized face. *Coal Sci Technol* 45(11):1–8 (in Chinese)
- Wang GF, Pang YH, Li MZ et al (2017b) Hydraulic support and coal wall coupling relationship in ultra large height mining face. *J China Coal Soc* 42(2):518–526
- Xu DJ, Peng SP, Xiang SY et al (2017) A novel caving model of overburden strata movement induced by coal mining. *Energies* 10(4):476
- Yang JZ (2017) Research on key mining technology of fully-mechanized working face with 8 m large mining height. *Coal Sci Technol* 45(11):9–14 (in Chinese)
- Yang SL, Wang JC, Yang JH (2017) Physical analog simulation analysis and its mechanical explanation on dynamic load impact. *J China Coal Soc* 42(2):335–343 (in Chinese)
- Zhang LH, Li NN (2017) Study on strata behavior law of fully-mechanized mining face with 8 m large mining height. *Coal Sci Technol* 45(11):21–26 (in Chinese)